Autonomous Robots (2024) 48:29
https://doi.org/10.1007/s10514-024-10176-2

BFAR: improving radar odometry estimation using a bounded false alarm rate detector

Anas Alhashimi[1,2] · Daniel Adolfsson[2] · Henrik Andreasson[2] · Achim Lilienthal[2,3] · Martin Magnusson[2]

Received: 30 September 2023 / Accepted: 31 August 2024 / Published online: 19 November 2024
© The Author(s) 2024

Abstract

This work introduces a novel detector, bounded false-alarm rate (BFAR), for distinguishing true detections from noise in radar data, leading to improved accuracy in radar odometry estimation. Scanning frequency-modulated continuous wave (FMCW) radars can serve as valuable tools for localization and mapping under low visibility conditions. However, they tend to yield a higher level of noise in comparison to the more commonly employed lidars, thereby introducing additional challenges to the detection process. We propose a new radar target detector called BFAR which uses an affine transformation of the estimated noise level compared to the classical constant false-alarm rate (CFAR) detector. This transformation employs learned parameters that minimize the error in odometry estimation. Conceptually, BFAR can be viewed as an optimized blend of CFAR and fixed-level thresholding designed to minimize odometry estimation error. The strength of this approach lies in its simplicity. Only a single parameter needs to be learned from a training dataset when the affine transformation scale parameter is maintained. Compared to ad-hoc detectors, BFAR has the advantage of a specified upper-bound for the false-alarm probability, and better noise handling than CFAR. Repeatability tests show that BFAR yields highly repeatable detections with minimal redundancy. We have conducted simulations to compare the detection and false-alarm probabilities of BFAR with those of three baselines in non-homogeneous noise and varying target sizes. The results show that BFAR outperforms the other detectors. Moreover, We apply BFAR to the use case of radar odometry, and adapt a recent odometry pipeline, replacing its original conservative filtering with BFAR. In this way, we reduce the translation/rotation odometry errors/100 m from 1.3%/0.4° to 1.12%/0.38°, and from 1.62%/0.57° to 1.21%/0.32°, improving translation error by 14.2% and 25% on Oxford and Mulran public data sets, respectively.

Keywords Radar · CFAR · Odometry · FMCW

1 Introduction

There is a great need for enabling mobile robots and self-driving cars to robustly operate in all seasons, weather, and visibility conditions. In contrast to cameras and lidars, FMCW radars are not affected by smoke, dust, rain or fog, and can detect obstacles regardless of visibility settings. Recently, radars, and especially spinning FMCW radars, have become compact, accurate and gained popularity and demonstrated more resilient localisation and mapping (Adolfsson et al., 2021, 2023; Hong et al., 2020). This makes them suitable for applications in harsh environments; e.g., underground mines (Brooker et al., 2007) and fire fighting (Mielle et al., 2019) tasks. Unfortunately, radars suffer from variable noise, multi-path and clutter reflections, ghost targets, and speckle noise which make target detection a challenging task (Zhou et al., 2022). Also, different applications require specialized detectors, for example, the problem of detecting moving targets in the sky using stationary radar is different from the problem of detecting stationary targets like buildings and trees in an urban area using the same sensor mounted over a moving vehicle.

In detection theory, CFAR, a family of adaptive threshold detectors for detecting targets in homogeneous noise, is usually suggested for a specified probability of false-alarm (P_{FA}).

✉ Anas Alhashimi
anas.alhashimi@coeng.uobaghdad.edu.iq

[1] Computer Engineering Department, University of Baghdad, Baghdad, Iraq

[2] Center for Applied Autonomous Sensor Systems (AASS), Örebro University, 70182 Örebro, Sweden

[3] School of Computation, Information and Technology, Technical University of Munich, Münich 80992, Germany

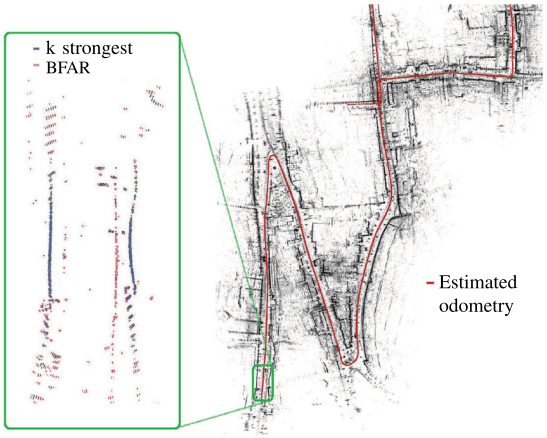


Fig. 1 The proposed radar detector, BFAR, offers superior detection quality compared to existing detectors and enhances radar odometry pipelines. It produces less noise than the *k strongest* (k = 12) method used in Adolfsson et al. (2021). The plots were generated using Oxford RobotCar data

Sadly, CFAR is not directly suitable for radar odometry estimation since we have complex background noise for radars that operate on ground level (Venon et al., 2022). Existing detectors for radar signals in odometry estimation applications either using ad-hoc detectors where most of them lack a clear interpretation of P_{FA} or over-simplify the detection process through proposing a fixed-level threshold that is sufficiently high to overcome the noise heterogeneity, which is easy to implement, but requires the knowledge of actual noise level to set the P_{FA}. A workaround is to use offline learning of the threshold level using manual optimization.

In this paper, we present a novel target detector, *bounded false-alarm rate (BFAR)*, that improves on existing radar filtering techniques in order to detect only *useful* and *highly-reflective* radar features by ignoring the ones with low power, even if they passed the adaptive threshold since they might be the result of speckle noise (see Fig. 1). It performs well with heterogeneous noise and features easy-to-tune parameters that are clearly related to P_{FA}. Conceptually, BFAR can be viewed as an optimized combination of CFAR and fixed-level thresholding designed to minimize odometry estimation error. The strength of this approach lies in its simplicity. We demonstrate the proposed BFAR filter on the previously existing pipeline for radar odometry, *conservative filtering for efficient and accurate radar odometry (CFEAR)* (Adolfsson et al., 2021), and show that by including BFAR we can decrease translation errors/100 m from 1.3%/0.4° to 1.12%/0.38° on Oxford data sets and from 1.62%/0.57° to 1.21%/0.32° on Mulran data set (an improvement of 14.2% and 25% respectively). To facilitate the replication of our training process and experimental results, we have made our code and datasets publicly available on GitHub (https://github.com/Anas-Alhashimi/CFEAR-BFAR).

The paper is organized as follows. Section 2 reviews related work. Section 3 outlines the problem formulation, provides details on the BFAR algorithm, explains the parameter learning procedure, Sect. 4 describes the evaluation procedure and the detection quality evaluation. Section 5 evaluates the detection performance in simulations and its application to radar odometry with real data. Finally, Sect. 6 presents the conclusions.

2 Related work

2.1 Radar-only odometry estimation

Previous methods for radar odometry overcome radar noise by learning to extract key points (Burnett et al., 2021; Barnes & Posner, 2020), remove noise (Aldera et al., 2019a, b; Barnes et al., 2020c; Burnett et al., 2021; Weston et al., 2022), leveraging motion constraints (Aldera et al., 2022), or by applying learning-free approaches that analyse intensity of radar measurements (Adolfsson et al., 2021; Cen & Newman, 2018, 2019; Hong et al., 2020; Kung et al., 2021; Park et al., 2020). Learning-free approaches for odometry were investigated by Hong et al. (2020), who extracted and matched SURF features; and Park et al. (2020), who proposed a method for dense matching of raw radar images. A similar dense matching technique was proposed by Barnes et al. (2020c), which additionally uses self-supervision from ground truth poses for learning to mask out noise. Unfortunately, the odometry quality is reduced when operating in environments that were not in the training set, despite using a large amount of training data. Kung et al. (2021) applied a fixed intensity threshold to discard weak, potentially spurious reflections. A more refined, though still ad-hoc, method, was successfully used by Adolfsson et al. (2021), which additionally bounds the number of returned reflections to improve efficiency. Cen and Newman (2018, 2019) investigated approaches for extracting features by analysing the intensity and gradients of the image.

As mentioned earlier, current detectors for radar signals in odometry estimation applications often rely on ad-hoc methods that do not provide a clear understanding of P_{FA}. Alternatively, other detectors tend to oversimplify the detection process by using a fixed-level threshold that is high enough to handle noise variability. This approach is easy to implement but requires knowledge of the actual noise level to set the P_{FA}. Our proposed detector addresses these issues.

2.2 Fixed-level detector

Some authors have used a simple fixed-level threshold instead of an adaptive method like CFAR (Hong et al., 2020; Kung et al., 2021; Mielle et al., 2019), however, selecting a suitable threshold value is not trivial. For example, Hong et al. (2020) extracted only peaks that are greater than a standard deviation of mean intensity per azimuth. Kung et al. (2021) suggests keeping all points exceeding a noise threshold, which needs to be learned offline. Adolfsson et al. (2021) showed that this can have a negative impact on efficiency and may have a negative impact on map quality. Other researchers suggested conservative filtering (Adolfsson et al., 2021; Marck et al., 2013). The most restricted one, used by Marck et al. (2013), keeps only the strongest reflection per azimuth, which will neglect a lot of potentially important information and good possible landmarks. Adolfsson et al. in CFEAR relaxed this condition, to instead keep the k strongest returns per azimuth, using values of $k = 6 \sim 12$ (Adolfsson et al., 2021). They presented good results in terms of translation and rotation errors on the Oxford public RobotCar dataset (Maddern et al., 2017). For this reason, and also to make the results directly comparable, we will use the same odometry estimation pipeline presented by Adolfsson et al. (2021, 2023) but replacing the k-strongest filter with our proposed detector, as well as with a fixed-level detector and a cell-averaging CFAR (CA-CFAR) detector for comparison purposes.

2.3 CFAR detector

The principle of CFAR was first described in 1968 by Finn (1968). They presented what is now known as CA-CFAR. Since then, CFAR has been extensively studied in the literature and many variants, more than 25 Machado-Fernández et al. (2017) have been proposed. The main idea behind CFAR is to estimate the background noise level for a certain sample (or cell) usually called called cell under test (CUT) in the middle of a sliding window, using statistics on neighboring samples inside the window (see Fig. 2). Then the detection threshold for that CUT is obtained after multiplying the estimated noise level by a constant calculated using a specified P_{FA}. After that, the window is slid by one sample, and the same procedure is applied to determine the threshold of the sample CUT+1, and so on until the end of the buffer is reached. This will give the advantage of an adaptive threshold that changes with background noise on the condition that all neighboring samples used in estimation are only generated from noise (i.e. containing no targets) which is hard to know before detection. Many variants of CFAR have been proposed to solve this problem. BFAR, however, is designed to tackle the problem of possible detections from noise due to complex noise structure, so it can be combined with most CFAR variants.

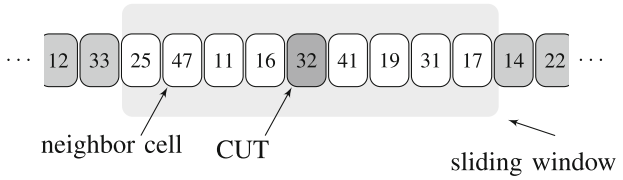


Fig. 2 The main idea behind CFAR is to estimate the noise at CUT using neighboring cells in a sliding window and use this estimated value to determine the threshold

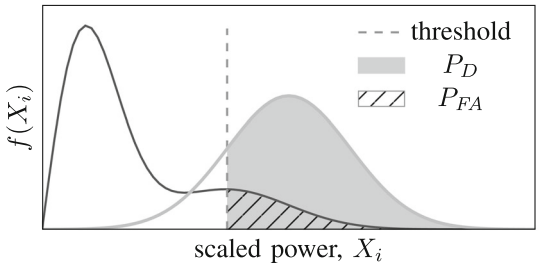


Fig. 3 Graphical representation of the P_{FA} and P_D, the shaded areas, for a single sample X_i. The black density is the PDF of X_i when there is only noise, while the gray density is the PDF of X_i when there is a target

We are not going to describe here existing CFAR variants but will focus on the main idea behind CA-CFAR and refer the interested readers to Machado-Fernández et al. (2017).

3 Methods

3.1 Problem formulation

The design of a detector is usually started by specifying the P_{FA}. The optimum detector is the one that maximizes the Probability of Detection (P_D) for a given P_{FA}. (See Fig. 3 for a graphical illustration). In a stationary noise environment, a fixed-threshold detector can achieve the optimum detector performance if the noise power is known. In practice, the noise power is not known, therefore a statistical estimator is used to estimate its value. Additionally, the noise is usually mixed with clutter (reflections from objects other than the target: buildings, trees, ground surface, etc; i.e., targets that are not in the exact direction that we currently consider) and therefore is nonstationary. For both reasons, the fixed-threshold is replaced by an adaptive detector, usually a CFAR variant, to have a controlled false-alarm rate (FAR).

In this paper, we present a new detection algorithm that is based on a different strategy than CFAR. It can handle the variable noise floor in a better way than the standard CFAR and does so by selecting a threshold from an affine transformation of the estimated noise level. In this setup, P_{FA} will depend on the unknown noise power, which might seem to be undesirable. However, its value will be controlled

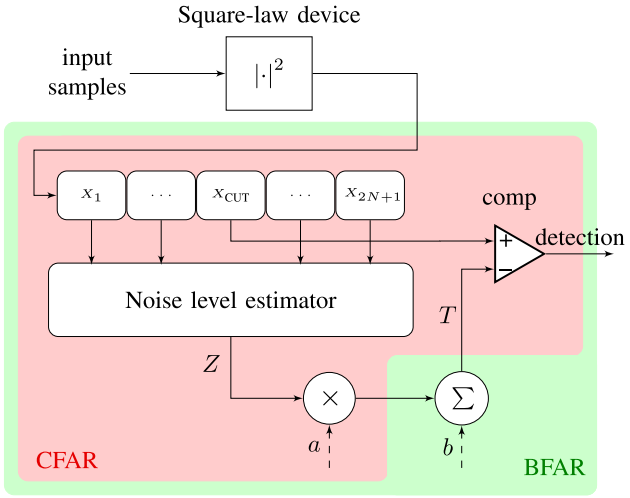


Fig. 4 The structure of BFAR detector. It is at a glance similar to CFAR but fundamentally different as it applies linear transformation on the estimated noise level. Notice that, in this manuscript, we always use four guard-samples, two on each side of X_{CUT} which are not shown in this figure to perceive the simplicity

in such a way that P_{FA} will decrease as the noise power is decreased, and increase with increased noise, but will not exceed a specified upper bound. Most importantly, this control is done automatically, as will be shown in Sect. 3 when deriving the P_{FA} equation.

In order to clarify the structure of BFAR, consider Fig. 4. We have two parameters $a, b \in \mathbb{R}$. The shaded area is common between classical CFAR and the proposed BFAR. Setting the parameter $b = 0$ will make the detector behave as CFAR. We assume the square-law device output is $X_k \in \mathbb{R}$, where k is an integer that represents the radar range-cell index. For clarity, a square-law device produces an output proportional to the square of its input signal. We are interested in finding the detection threshold T for X_{CUT} given N samples before it and another N samples after it. Usually, there are one or more *guard-cells* after and before the N samples close to X_{CUT} (removed from Fig. 4 for clarity). The CFAR detector estimates the expected level of background noise at X_{CUT} from the $2N$ neighboring cells. For example, the *noise level estimator* in CA-CFAR is a simple sum and the noise level is calculated by averaging the $2N$ samples, which gives $\bar{Z} = \frac{Z}{2N}$. The comparator output will register a target when the level of X_{CUT} exceeds the threshold T, where $T = aZ$. The parameter a is calculated according to the required P_{FA} and N.

The threshold in BFAR for X_{CUT} is then

$$T = a \times Z + b. \tag{1}$$

The affine transformation will not give a constant FAR but will give FAR that is bounded from above—hence the name BFAR (see plots in Fig. 5). Learning the best values for the parameters can be done using grid search on a training dataset (as demonstrated in Sect. 3.3). We assume here the values of a and b are fixed during the estimation process. Notice that in Fig. 4 the *noise level estimator* block is generic, therefore it is possible to apply the BFAR structure to most CFAR variants by plugging in the corresponding noise estimation block without further modifications.

In Sect. 5.2 we show quantitative results on the Oxford Radar RobotCar dataset and demonstrate that CFEAR radar odometry [specifically, the computationally efficient variant in Adolfsson et al. (2021)] with BFAR detection instead of k-strongest can reduce the odometry error by 12%.

3.2 BFAR mathematical derivation

In this section, we will give the derivation of P_{FA} for our proposed BFAR detector. We will assume the cell-averaging noise estimation in Fig. 4 for simplicity and comparison purposes with CA-CFAR.

1. Assuming independent and Gaussian noise, then the output of the square-law device X_i will be exponentially distributed and independent, with PDF

$$f(X_i) = \frac{1}{2\lambda} \exp\left(\frac{-X_i}{2\lambda}\right), \quad x \geq 0 \tag{2}$$

and

$$\lambda = \begin{cases} \mu, & \text{under } \mathrm{H}_0 \\ (S + \mu), & \text{under } \mathrm{H}_1 \end{cases} \tag{3}$$

where

- H_0 is the null hypothesis of no target, so X_i contains only noise,
- H_1 is the alternative hypothesis of the presence of a target,
- μ is the total background clutter-plus-thermal noise power, its value is not fixed and is changing from cell-to-cell according to an unknown but continuous and smooth function (no fast changes are expected),
- S is the average signal power of a target and signal-to-noise ratio (SNR) $:= S/\mu$.

2. The detector performance is determined by the average detection and false alarm probabilities. Following the same procedure in Gandhi and Kassam (1988), the P_{FA} is (see also Fig. 3)

$$P_{FA} = \mathbb{E}\left[p\left(X_{\text{CUT}} > aZ + b \,|\mathrm{H}_0\right) \mid Z\right] \tag{4}$$

$$P_{FA} = \mathbb{E}\left[\int_{aZ+b}^{\infty} \frac{1}{2\mu}\exp\left(\frac{-y}{2\mu}\right) dy\right] \tag{5}$$

$$= \mathbb{E}\left[\exp\left(-\frac{aZ+b}{2\mu}\right)\right] \tag{6}$$

$$= \mathbb{E}\left[\exp\left(-\frac{aZ}{2\mu}\right)\right]\mathbb{E}\left[\exp\left(\frac{-b}{2\mu}\right)\right] \tag{7}$$

$$= M_Z\left(\frac{a}{2\mu}\right)\exp\left(\frac{-b}{2\mu}\right) \tag{8}$$

where $M_Z(\cdot)$ denotes the moment generating function (MGF) of the random variable Z.

3. For a *cell-averaging* processor operating on $2N$ samples,[1] the random variable Z will be

$$Z := \sum_{i=1}^{2N} X_i \tag{9}$$

where X_i are the samples of the neighboring cells. From Gandhi and Kassam (1988), the distribution of Z will be

$$Z \sim \Gamma\left(2N, 2\mu\right), \tag{10}$$

and the corresponding MGF is

$$M_y(u) = (1 + 2\mu u)^{-2N}.$$

Substituting this in Eq. (8) above, we obtain

$$P_{FA} = (1+a)^{-2N}\exp\left(\frac{-b}{2\mu}\right). \tag{11}$$

Setting the parameter $b = 0$, Eq. (11) will be reduced to

$$P_{FA} = (1+a)^{-2N} \qquad \text{for } b = 0 \tag{12}$$

which is exactly the P_{FA} equation for CA-CFAR, [the expression and derivation in Gandhi and Kassam (1988)]. Setting $a = 0$ will give

$$P_{FA} = \exp\left(\frac{-b}{2\mu}\right) \qquad \text{for } a = 0 \tag{13}$$

which is the P_{FA} for a fixed-level detector. So BFAR with *cell-averaging* can be seen as a generalization for the classical CA-CFAR detector. The smaller values of μ compared to b correspond to a smaller exponential term in (11) which makes the value of P_{FA} even smaller. On the other hand, large values of μ compared to b make the exponential term closer to one and the P_{FA} simplifies to

$$P_{FA} \approxeq P_{FA_{ub}} := (1+a)^{-2N} \tag{14}$$

which is the false-alarm upperbound (P_{FAub}). Then we rewrite (11) as

$$P_{FA} = P_{FA_{ub}}\exp\left(\frac{-b}{2\mu}\right). \tag{15}$$

When the parameter $a = 0$, both P_{FA} and P_D will be directly related to the background noise level μ.

4. In a similar way, we derive an expression for P_D:

$$P_D = \mathbb{E}\left[p\left(X_{\text{CUT}} > aZ + b\,|\mathrm{H}_1\right) \mid Z\right]$$

$$= \left(1 + \frac{a}{S/\mu + 1}\right)^{-2N}\exp\left(\frac{-b}{2\left(S+\mu\right)}\right). \tag{16}$$

The first term corresponds to P_D of a CA-CFAR detector, while the last term corresponds to P_D of a fixed-level detector. The exponential term in (16) will indeed reduce P_D compared to CA-CFAR. We plot Eqs. (15) and (16) in Fig. 5 with several values of the parameter b to clarify this relation. The P_{FA} is increased with increased noise, but will not exceed the bounds. The equations suggest that the P_D depends on both signal and noise power. For that reason, we have two graphs, one with S fixed and one with μ fixed. The value of P_D in BFAR decreases compared to that of CA-CFAR as the parameter b increases.

3.3 Parameter learning

It is clear from (11) that we need to tune the two parameters a and b for the detector, which is not straightforward, especially because the value of μ is not known. Therefore, we propose the following procedure to learn them from a preset number of samples N and P_{FAub}:

- First, with a specified value of N and a given P_{FAub}, the parameter a can be computed using Eq. (14). This involves substituting the known values into the equation and solving for a, ensuring that the false alarm bound will not be exceeded.
- Second, the parameter b can be determined through a data-driven approach. Specifically, b can be learned from a dataset that is relevant to the specific use case. In the context of this paper, which focuses on radar odometry, we utilize a training dataset that includes ground-truth pose information obtained from GNSS (Global Navigation Satellite System). To accurately estimate b, we

[1] Here we are considering the CA-CFAR for simplicity only. Please note that any other processors like Ordered Statistics CFAR (OS-CFAR), Trimmed Mean CFAR (TM-CFAR), etc. can be used in the same way.

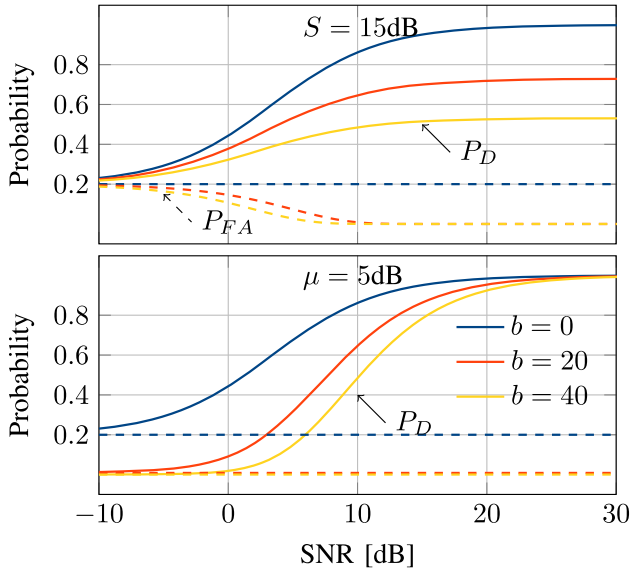


Fig. 5 The BFAR detection and false-alarm probabilities versus SNR. The upper plot shows the relations of the probabilities P_D (16), in the solid lines, and P_{FA} (15), in the dashed lines, against μ for fixed $S = 15$, with $P_{FA_{ub}} = 0.2$ and $a = 1$. The lower plot shows how P_D changes with signal power S for a fixed noise value $\mu = 5$. Notice that P_{FA} here is always fixed and independent on S according to (15). Recall that for $b = 0$ the detector is CA-CFAR which maintains a constant probability of false alarms, while BFAR has a lower P_{FA} as the SNR increases at the cost of a lower P_D. The blue curve is identical in both, since for $b = 0$ it will be CA-CFAR where P_D depends only on signal-to-noise power ratio

employ a grid search method, which involves systematically searching through a predefined set of potential values for b and selecting the one that optimizes odometry performance based on the training data (see Fig. 13).

Finally, we use the obtained parameter values in our detection algorithm for radar data.

4 Evaluation methods

4.1 Odometry estimation evaluation

To evaluate and examine the performance of BFAR, we include it in the recent radar odometry pipeline CFEAR (the version presented in Adolfsson et al. (2021)) as depicted in Fig. 6. CFEAR is an efficient and accurate pipeline for incremental pose estimation that operates on 360° spinning radar data, producing state-of-the-art accuracy in odometry drift. It extracts features in a two-step approach that first applies a conservative filter in polar space, keeping the k strongest returns for each azimuth angle, and then computes a sparse set of oriented surface points in Cartesian space. The sparse set of surface points is registered jointly to a history of key

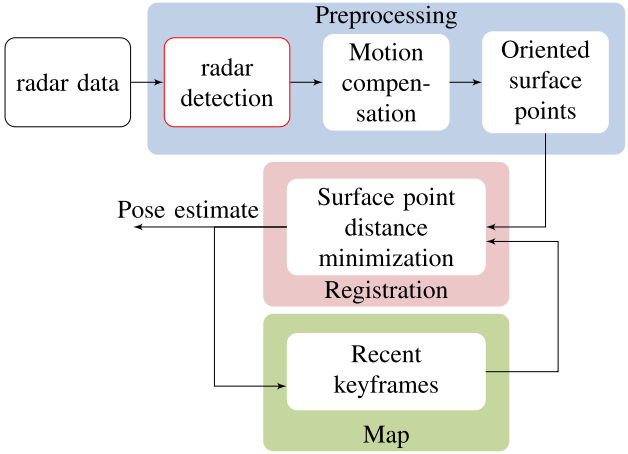


Fig. 6 Overview of CFEAR radar odometry, used for evaluating BFAR radar detection. In the previously published version of CFEAR (Adolfsson et al., 2021), the *radar detection* block uses a k-strongest detector. We replace this block with BFAR and show how it leads to a new state-of-the-art in radar odometry

frames in order to estimate the pose and velocity of the radar. The estimated velocity is used to perform motion compensation. In the original publication (Adolfsson et al., 2021), CFEAR radar odometry was optimized to be fast and efficient, using a conservative k-strongest filter (with $k = 12$ detections per azimuth) that typically removes secondary landmarks combined with a fixed-threshold to prevent detections from noise when only few targets exist. Other values of k have been evaluated in the recent publication (Adolfsson et al., 2022). For that reason, the conservative filter can be replaced with our proposed filter, which produces improved detections compared to the conservative filter, and can additionally aid odometry estimation as demonstrated in Sect. 5.

4.2 Detection quality evaluation

In addition to using odometry accuracy as a measure of detection performance (assuming that a good detector produces stable landmarks that are suitable for odometry), we have also evaluated detection quality by measuring detection stability and repeatability. Those measures, which originate from computer vision, have previously been used to analyse the detection quality in lidars (Kallasi & Rizzini, 2016; Nielsen & Hendeby, 2023; Usman et al., 2019).

4.2.1 Global detector stability test

The uncertainty of a detected target is inversely related to its reflected power. Hence, the average power of detections is a measure of global detector stability.

Detector repeatability

Detector repeatability is the standard procedure in image processing to assess key-point feature detector performance (Tuytelaars & Mikolajczyk, 2008). Assuming correct associations (geometric only), the repeatability is defined as the ratio of commonly detected targets in reference and source images over the smaller of the two target sets (Boroson & Ayanian, 2019). Assume $|\kappa_i|$ and $|\kappa_{i+1}|$ are the number of detections in the reference and source images, then the relative repeatability $\mathcal{R}$ is

$$\mathcal{R}_i := \frac{|\kappa_i \cap \kappa_{i+1}|}{\min(|\kappa_i|, |\kappa_{i+1}|)} \tag{17}$$

where the operation $A \cap B$ stands for common detections between the two images A and B. In case we have k images, the average repeatable detections will be

$$\overline{\mathcal{D}} := \frac{1}{k-1} \sum_{i=1}^{k-1} |\kappa_i \cap \kappa_{i+1}| \tag{18}$$

and the average relative repeatability will be

$$\overline{\mathcal{R}} := \frac{1}{k-1} \sum_{i=1}^{k-1} \mathcal{R}_i \tag{19}$$

Bias in repeatability rate

This repeatability measure (19) is biased toward detectors that return more detections from the same target (redundant detections). This was studied and explained with lidar sensors in Rey-Otero et al. (2015) and Rey-Otero and Delbracio (2015). As an example, suppose we have 2 detections: one from a target and another from noise. This gives a repeatability rate of 0.5. Another detector may return 9 detections from the same target and one from noise, yielding a higher repeatability rate of 0.9. However, it is important to note that the superiority of this detector is not guaranteed, as the detections it generates may be redundant, all pertaining to the same target. In fact, if we take into account memory and processing power constraints, it could potentially yield worse results. Therefore, our deduction leads us to the best detector being the one that yields a higher number of *stable* and *repeatable* detections while *avoiding redundancy*.

In order to accurately compare the performance of different detectors, we must first identify the optimal parameter set for each detector type. This will ensure that all detectors are evaluated under fair conditions, taking into account the difficulty of parameter tuning or learning, if necessary. Once the optimal parameter set has been identified, we can then compare the performance of the different detectors given their optimized parameters.

Given the above measures and the various detectors we are considering here (fixed-threshold, k-strongest, CFAR, and BFAR), we are expecting fixed-threshold detectors to have higher repeatability compared to adaptive threshold ones due to redundancy. Also, the k-strongest is expected to have higher global detector stability since it is designed to choose the strongest returns and is also expected to have the lowest detection from noise compared to others. BFAR is expected to have less redundant detections due to its adaptive nature and also to have fewer detections from noise, compared to CA-CFAR, due to the added offset level.

5 Simulations and experimental validation

5.1 Detection performance, in simulation

Since the available datasets that use scanning FMCW radar in a robotics context (Barnes et al., 2020a; Kim et al., 2020) do not include *detection* ground-truth (i.e., labels of which radar points correspond to true targets vs. noise), we carried out extensive simulations to evaluate BFAR performance with both homogeneous and heterogeneous background noise. Those simulations do not cover all the artifacts that exist in FMCW radar signal, which is complex and not easy to simulate (Weston et al., 2021), but actually focus on noise heterogeneity and variable target width. We simulate homogeneous background noise using $\lambda = \mu$ as described in (3). For heterogeneous background noise, we model it as an exponentially distributed random variable where its parameter, λ in (2) is a scaled discrete uniform random variable, takes 5 discrete values between μ and 10μ. We used an exponentially distributed random variable also to simulate targets, but with fixed parameter $\lambda = S + \mu$ (Swerling I model). In all simulations, unless specified otherwise in the caption, the target width occupies a random range of 1 to 20 cells. We simulate a radar beam of 10,000 samples containing 100 targets randomly displaced with uniform distribution. Each point on the following simulation plots is obtained by averaging the results of 100 beams.

We plotted simulation results for operational P_{FA} and P_D in Fig. 7, for homogeneous and heterogeneous noise respectively, with the same values of b in Fig. 5 to compare easily. We calculated the optimum threshold using the true value of noise parameter at each cell and the desired P_{FA} of 0.2.

The top plot in Fig. 7a looks quite similar to Fig. 5, while the bottom plot shows reduced P_D due to the variable target width. Notice there is a small decrement in P_{FA} with increased signal power. This reduction is due to the presence of high power target in the estimation window as discussed in Sect. 2.3, since the increased target power results in increased

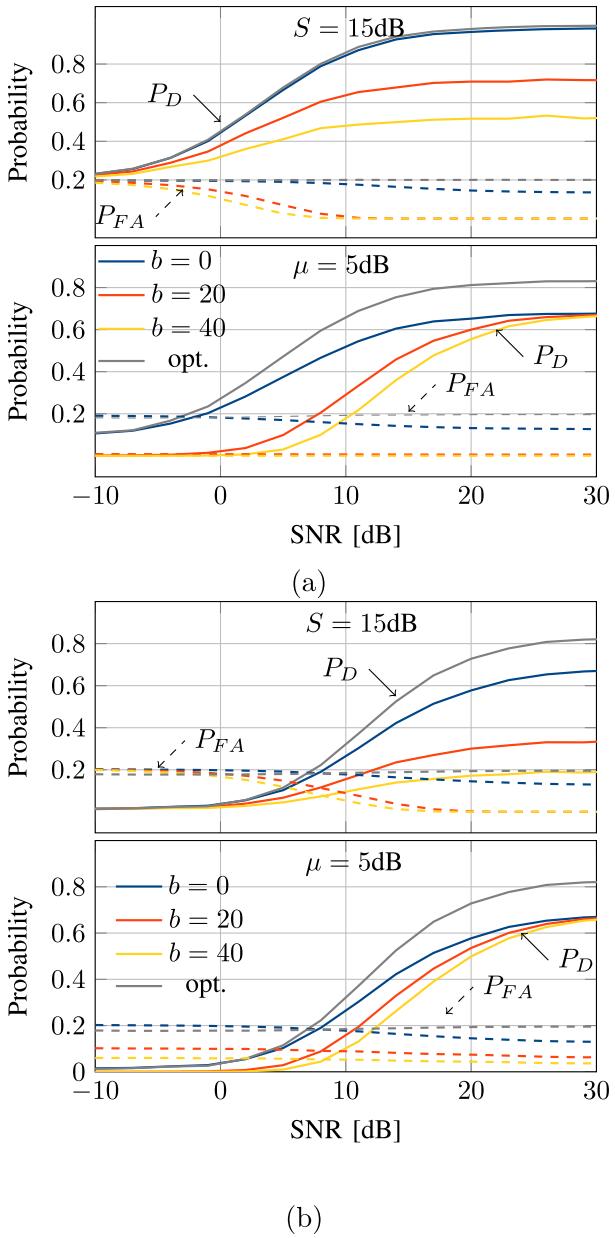


Fig. 7 Simulation results for operational false alarm and detection probabilities are presented for cases with variable target width: **a** homogeneous noise, and **b** heterogeneous noise. The gray lines correspond to the optimum detector at $P_{FA} = 0.2$

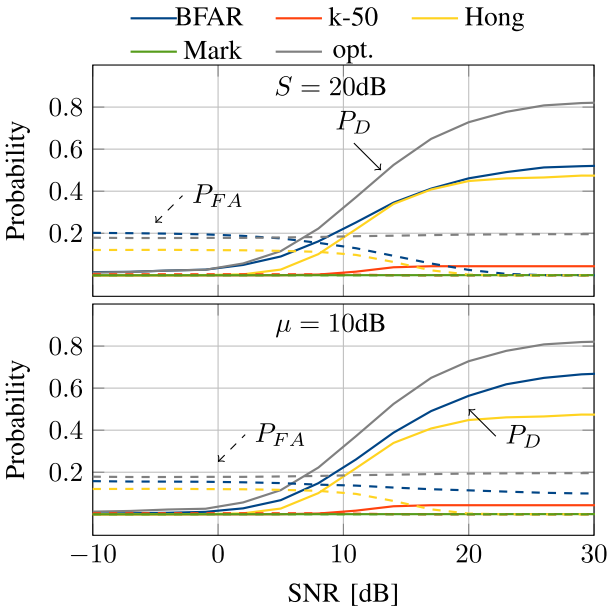


Fig. 8 Simulation results for comparing operational false alarm P_{FA} and detection probabilities P_D of BFAR with other detectors affected by heterogeneous noise and variable target width

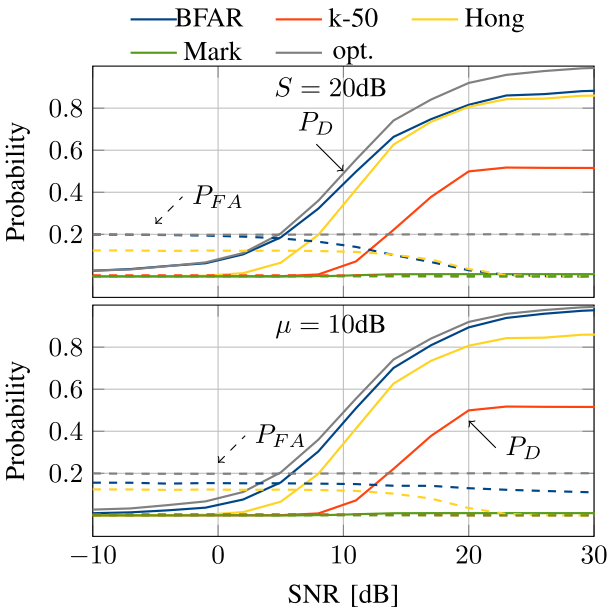


Fig. 9 Simulation results for comparing operational false alarm and detection probabilities of BFAR with other detectors affected by heterogeneous noise and one sample target width

average and then increased threshold which in turn reduces the P_{FA}. In the heterogeneous noise case (Fig. 7b), the P_D is reduced for both plots.

We conclude from those plots that the P_D is reduced in general with the increased value of parameter b and the P_{FA} is always equal or smaller than the specified bound as expected from (15).

We also used simulations to compare the performance of BFAR (with $b = 20$) under heterogeneous noise and variable target width against other detectors; k-strongest with $k = 50$ (Adolfsson et al., 2021), fixed-level of mean plus standard deviation (Hong et al., 2020), only the strongest target (Marck et al., 2013), and the optimum detector. The results obtained are presented in Fig. 8 for variable target width and Fig. 9 for one sample target width. We conclude from those figures that BFAR outperforms other detectors in

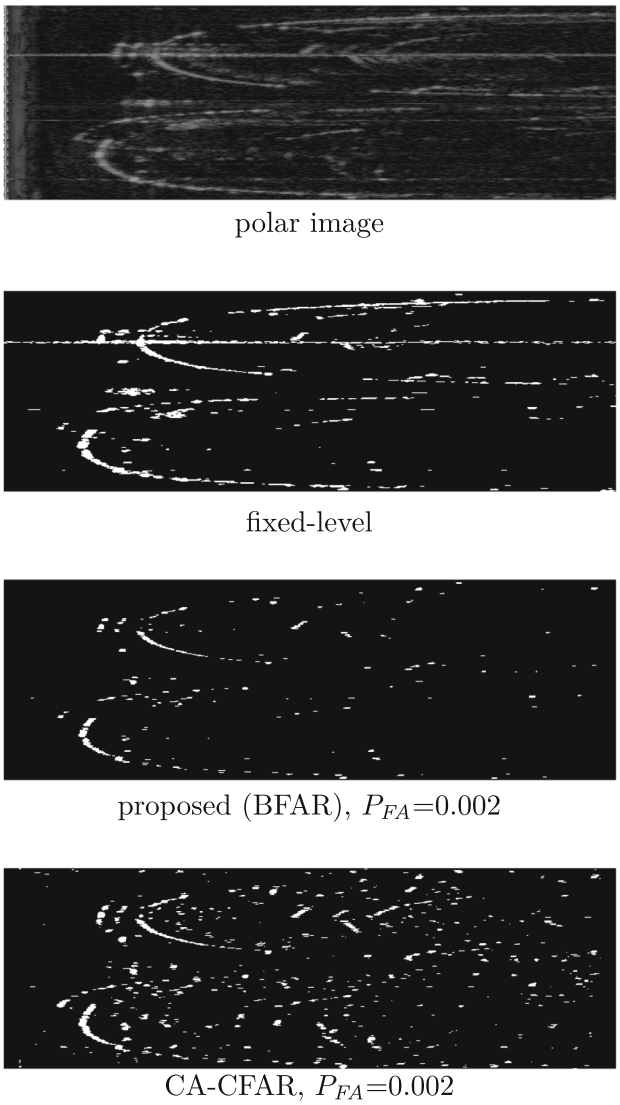


Fig. 10 This figure illustrates an example of the enhanced detection capability of the proposed method compared to other detectors. The top image displays the original polar image, while the subsequent images show the detection results from the fixed-level detector, BFAR, and CA-CFAR, respectively



Fig. 11 The constructed radar map during one of the simulations on Mulran dataset, sequence DCC03

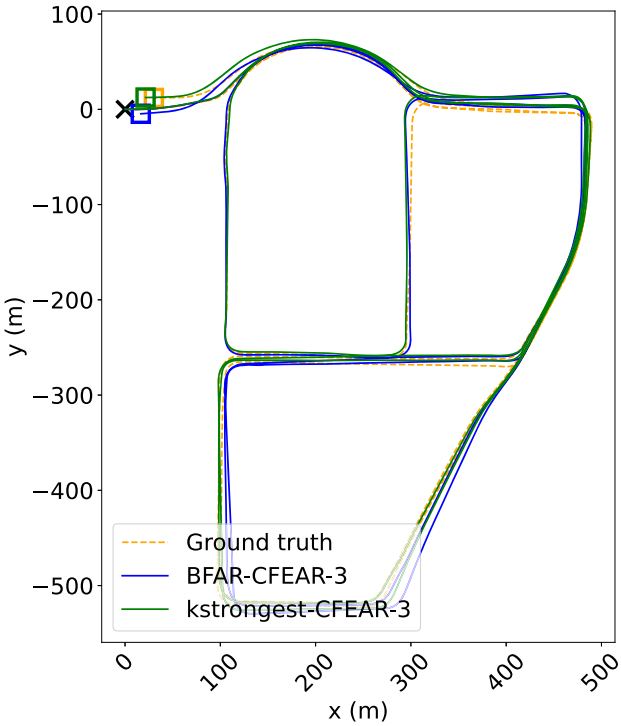


Fig. 12 The estimated trajectory during one of the simulations on Mulran dataset, sequence DCC03

P_D and also that variable target width greatly reduces the detection performance.

5.2 Application to radar odometry, with real data

We investigated the performance of the proposed detection algorithm in odometry estimation using the Oxford Radar RobotCar dataset (Barnes et al., 2020a; Maddern et al., 2017) since it is a relevant use case where there is a lot of recent interest and to facilitate the evaluation on a large data set. Figure 10 showcases an example of the original polar radar image alongside three different filtered images. The BFAR method successfully removes ghost targets (the horizontal white line seen in the fixed-level image) and reduces the number of noisy detections (the small scattered dots evident in the last image). As indicated above, no ground truth labels for real landmarks/noise are available. However, ground-truth poses are provided, enabling evaluation on odometry quality. The data set contains both raw radar data and ground-truth information for odometry.

The evaluation is performed using the standard odometry benchmark from KITTI (Geiger et al., 2012) to compute the following performance metrics:

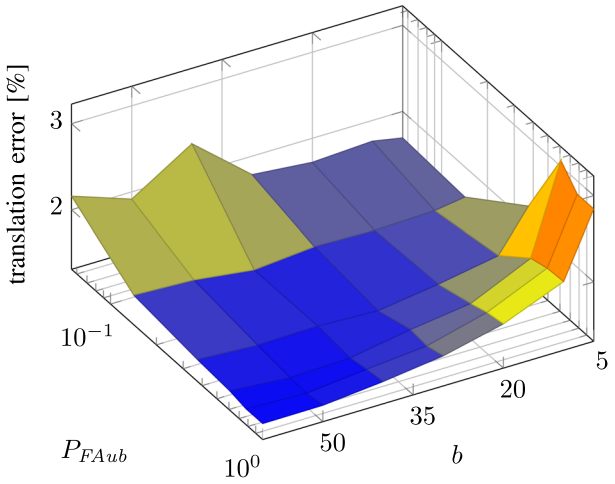


Fig. 13 Translation error surface with P_{FAub} and b for $N = 20$. Used for parameter learning in the Oxford dataset

- Average sub-sequence translational and rotational errors, by evaluating possible sub-sequences of length (100, 200, . . ., 800) m.
- Absolute trajectory error (ATE): the root-mean-square error (RMSE) between estimated poses and corresponding ground truth.

5.3 Odometry estimation performance

To learn the offset parameter b, we select one sequence from the dataset (14-50-05) for learning only. With $N = 20$ and parameter grid $a = [0, 0.1, 0.25, 0.5, 1, 2, 3]$, $b = [5, 10, 15, 20, 30, 40, 50, 60]$, we record the odometry metrics to find the best value for the parameters. As stated above, since N is fixed, the values of P_{FAub} can be computed directly from a to be [1, 0.9, 0.78, 0.61, 0.37, 0.14, 0.06]. The smallest translation error, rotation error and ATE achieved during this grid search corresponds to $a = 0.5$ or $P_{FA_{ub}} = 0.61$ and $b = 45$ in the training dataset. See grid plot in Fig. 13 and error curves in Fig. 14.

We apply the learned and optimized parameters, $a = 0.5$ and $b = 45$, and insert BFAR in the CFEAR odometry pipeline for evaluation on the remaining sequences of the RobotCar dataset. Except for the detector, we used the same parameters of CFEAR as in the original publication (Adolfsson et al., 2021).

The obtained odometry errors are presented in Table 1 and compared to three recent radar odometry baselines, as well as one baseline using lidar odometry for reference. To enhance the generalization of parameter learning, we employed distinct environments for learning and testing. Specifically, we used the parameters learned from the Oxford dataset to perform odometry estimation on the Mulran dataset (Kim et

Table 1 Evaluation of 8 sequences with different methods and sensor modalities on the Oxford radar RobotCar dataset (Barnes et al., 2020b)

Method	res	Sequence							Mean
		10-12-32	16-13-09	17-13-26	18-14-14	18-15-20	10-11-46	16-11-53	18-14-46	
CFEAR-3-BFAR (ours)	0.043	***1.07/0.35***	**1.13/0.37**	***1.08/0.37***	**1.14/0.39**	**1.08/0.39**	***1.09/0.38***	***1.19/0.39***	***1.17/0.39***	1.12/0.38
CFEAR-3 (Adolfsson et al., 2023)	0.043	1.23/0.36	1.25/0.39	1.25/0.40	1.34/0.41	1.26/0.41	1.26/0.39	1.42/0.39	1.42/0.44	1.31/0.40
CFEAR-BFAR (ours)	0.043	***1.48/0.42***	**1.54/0.43**	***1.52/0.44***	**1.49/0.45**	**1.45/0.44**	***1.54/0.45***	***1.65/0.49***	***1.65/0.50***	1.54/0.45
CFEAR-k12 (Adolfsson et al., 2021)	0.043	1.64/0.48	1.86/0.52	1.66/0.48	1.71/0.49	1.75/0.51	1.65/0.48	1.99/0.53	1.79/0.5	1.76.0.50
Hong odometry (Hong et al., 2020)	0.043	2.98/0.8	3.12/0.9	2.92/0.8	3.18/0.9	2.85/0.9	3.26/0.9	3.28/0.9	3.33/1	3.11/0.9
Hero (Burnett et al., 2021)	0.2628	*1.77/0.62	*1.75/0.59	*2.04/0.73	*1.83/0.61	*2.20/0.77	*2.14/0.71	*2.01/0.61	*1.97/0.65	1.96/0.66
SuMa (Lidar)	N/A	1.1/0.3	1.2/0.4	1.1/0.3	0.9/0.1	1.0/0.2	1.1/0.3	0.9/0.3	1.0/0.1	1.03/0.3
(Behley & Stachniss, 2018)										

Results are given in % translation error/deg/100 m. "*" indicates that the results are not exactly comparable due to lacking spatial cross-validation
The values in bold correspond to the smallest value in the column The bold formatting represents CFEAR-3-BFAR, and the bold italic formatting represents CFEAR-BFAR

Table 2 We evaluated nine sequences from the Mulran dataset (Kim et al., 2020) using parameters learned from the Oxford dataset

Method	res.	Sequence								Mean
		KAIST01	KAIST02	KAIST03	DCC01	DCC02	DCC03	RIV01	RIV02	RIV03	
SuMa Full	0.0583	2.9/0.8	2.64/0.6	2.17/0.6	2.71/0.4	4.07/0.9	2.14/0.6	1.66/0.6	1.49/0.5	1.65/0.4	2.38/0.5
LOAM[b]	–	2.70/0.82	2.80/0.84	7.54/0.79	3.16/0.86	2.64/0.74	2.23/0.74	4.25/0.88	4.14/0.90	4.21/1.02	3.74/0.84
RadarSLAM-Full[c]	0.0583	1.75/0.5	1.76/0.4	1.72/0.4	2.39/0.4	1.90/0.4	1.56/0.2	3.40/0.9	1.79/0.3	1.95/0.5	2.02/0.4
RadarSLAM-odometry[d]	0.0583	2.13/0.7	2.07/0.6	1.99/**0.5**	2.70/0.5	1.90/0.4	1.64/0.4	2.04/0.5	1.51/0.5	1.71/0.5	1.97/**0.5**
CFEAR-1-BFAR (ours)	0.0595	***1.17/0.34***	1.18/0.36	***1.18/0.57***	***2.11/0.29***	***1.28/0.23***	***1.18/0.25***	***1.33/0.36***	***1.11/0.31***	***1.39/0.26***	1.32/0.33
CFEAR-1	0.0595	2.62/0.97	2.45/0.90	2.85/1.08	2.73/0.73	1.82/0.60	1.77/0.62	2.55/0.90	2.71/0.82	3.56/0.82	2.56/0.83
CFEAR-3-BFAR (ours)	0.0595	**0.99/0.31**	**1.08/0.33**	**1.10/0.56**	**1.98/0.31**	**1.16/0.24**	**1.04/0.25**	**1.32/0.36**	**1.03/0.33**	**1.22/0.23**	1.21/0.32
CFEAR-3	0.0595	1.59/0.66	1.62/0.66	1.73/0.78	2.28/0.54	1.49/0.46	1.47/0.48	1.59/0.63	1.39/0.51	1.41/0.40	1.62/0.57

The values in bold correspond to the smallest value in the column The bold formatting represents CFEAR-3-BFAR, and the bold italic formatting represents CFEAR-BFAR
The results, presented as (% translation error/deg/100 m), are compared with those from various state-of-the-art methods. Our proposed method consistently outperforms all others
[a]Behley and Stachniss (2018)
[b]Zhang and Singh (2017)
[c]Hong et al. (2021)
[d]Hong et al. (2021)

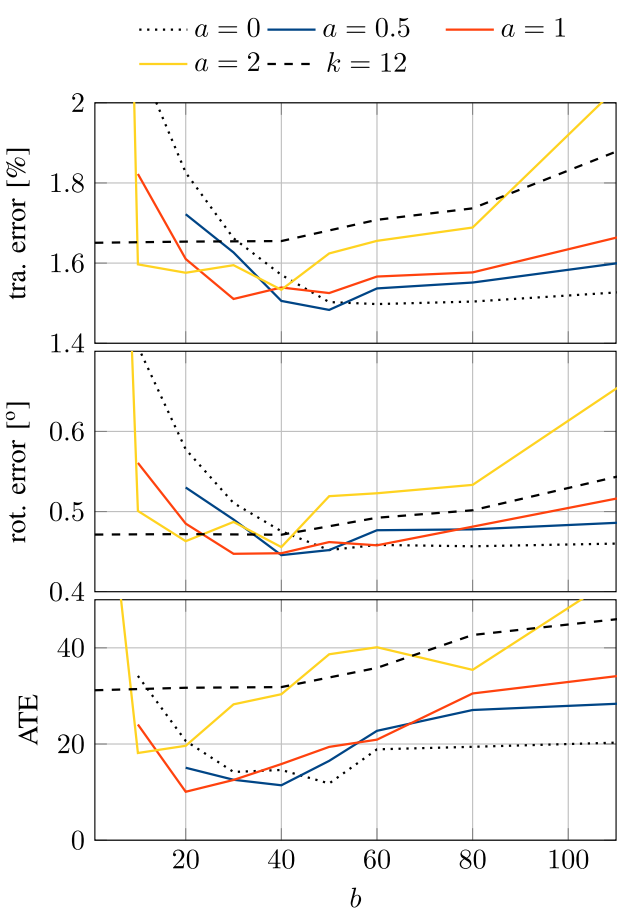


Fig. 14 Estimation evaluation metrics versus threshold parameter b for different detectors. BFAR performs better than $k = 12$ in general and also better than fixed-level threshold when $b < 50$

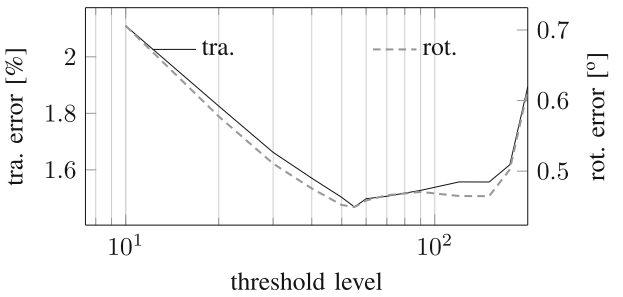


Fig. 15 Estimation evaluation metrics of fixed-level detector against threshold level (b when $a = 0$)

al., 2020), which was recorded in different geographical locations and using different sensors. Table 2 presents the odometry evaluation results, demonstrating that our algorithm surpasses the latest state-of-the-art outcomes.

Compared to the state of the art, CFEAR with BFAR detection consistently has smaller errors over all the trajectories, which indicates that the key-frames are consistent and fewer false detections are provided.

To provide readers with a clearer understanding of the proposed method's performance and capabilities, Fig. 12 displays the constructed radar map from DCC03 sequence of Mulran dataset and Fig. 11 presents the corresponding estimated trajectory. The Fig. also includes the estimated trajectory using the *k strongest* filtering for easy comparison.

5.4 Odometry estimation performance compared to fixed-level and CA-CFAR

In addition to comparing BFAR with the original k-strongest detection module of the CFEAR odometry pipeline, we also compute the odometry results of CFEAR using a fixed-level and CA-CFAR detector. It was not possible to set the value of P_{FA} because we don't know the actual noise level, so we performed a grid search starting from 0 and reporting the useful values of the threshold with corresponding estimation metrics as depicted in Fig. 15. Small threshold values result in more false-detections and hence worse odometry estimation, while large values result in fewer detected features, which also degrade the estimation. The best performance indexes were obtained with threshold-level around 55. This is equivalent to BFAR in (1) with $a = 0$ and $b = 55$. Then we run the odometry estimation pipeline with BFAR detector.

Figure 16 shows the plots of the different evaluation metrics vs P_{FAub} with parameter b. Notice that in the case of $b = 0$ (blue curves), the detector will be CA-CFAR and P_{FAub} is exactly equal to P_{FA} values. Comparing BFAR with CFAR, we can see that BFAR works well even with P_{FAub} close to one. Comparing this with the limited selection of P_{FA} in CA-CFAR, proves the flexibility in parameter selection and also the ability to automatically account for changes in background noise level. Notice that, for $P_{FAub} = 1$ ($a = 0$), BFAR is equivalent to a fixed-level detector.

Even though a fixed-level detector may work well for certain threshold levels, there is no information about the operational P_{FA} because of the unknown and possibly changing background noise (see (13)). So, unlike CA-CFAR, both BFAR and fixed-level detectors can handle complex noise given a learned parameter for tuning the threshold, but BFAR has the advantage of limiting the upper bound for P_{FA}. On the other hand, CA-CFAR does not require parameter learning but suffers from bad performance with complex noise and requires precise selection of P_{FA} within a tightly limited range to prevent the estimation pipeline from fail and hence requires offline parameter tuning.

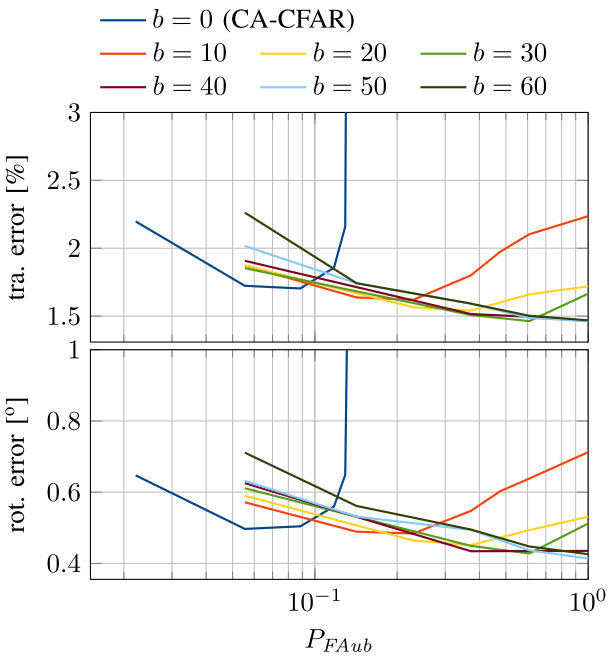


Fig. 16 BFAR estimation evaluation metrics versus the P_{FAub}. BFAR is less sensitive to parameter tuning, and provides lower odometry error, than CA-CFAR

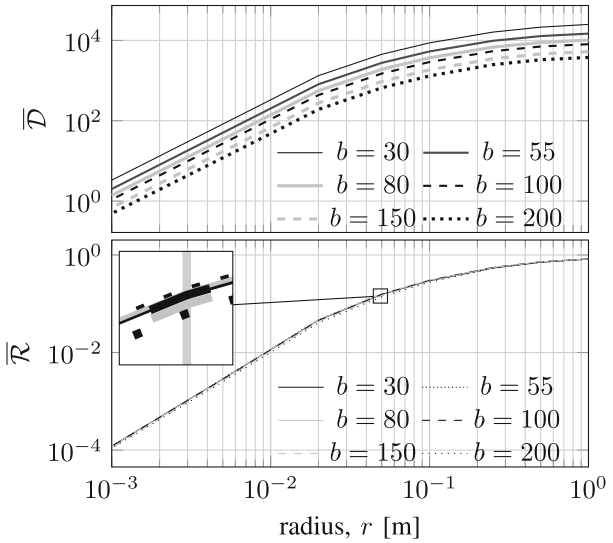


Fig. 17 Average repeatable detections (top) and average relative repeatability (bottom) vs. search radius r and with a threshold as a parameter for the fixed-level detector. The number of repeatable detections is increased with decreased threshold levels while relative repeatability is approximately the same, which indicates redundant detections

5.5 Repeatability tests

We also report the relative repeatability scores using the same dataset and parameter values. We computed similar detections by transforming the destination image using the available ground-truth and compute for each detected point in the source the closest detected point in the destination that lies inside a circle of radius r (closest in the sense of geometrical distance). Figure 17 shows the average repeatable detections and the average relative repeatability vs. the search radius r for the fixed-level detector with different values of

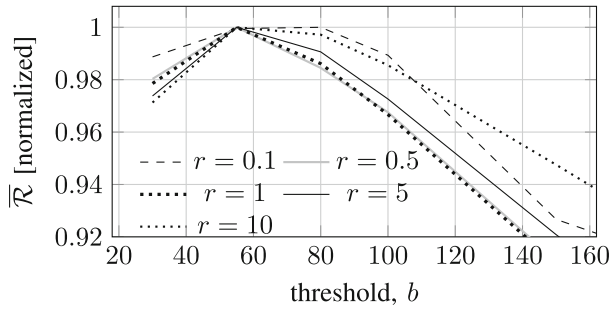


Fig. 18 Normalized relative repeatability vs. threshold level with searching radius r (in cm) as parameter. The curves are normalized to have max value of 1 for sake of visibility. There is an agreement between estimation performance plots Fig. 15 and normalized repeatability plots Fig. 18 to have the best scores at threshold levels slightly greater than 50, independent on r

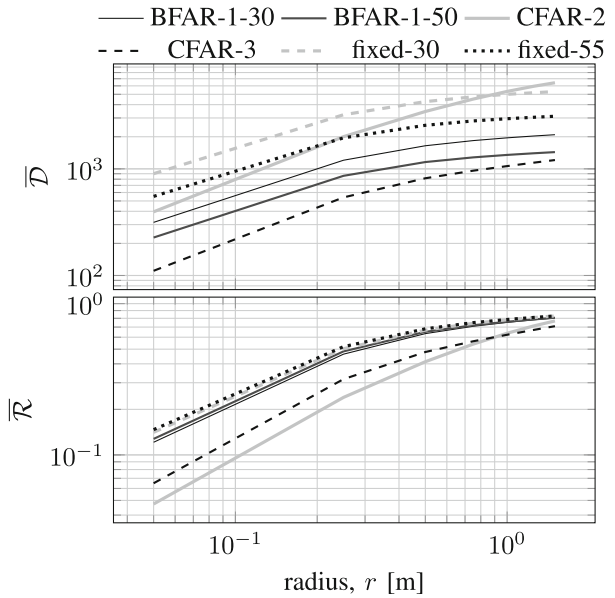


Fig. 19 Top: average repeatable detections per radar scan vs. searching radius r. Bottom: average relative repeatability vs. r for different detectors

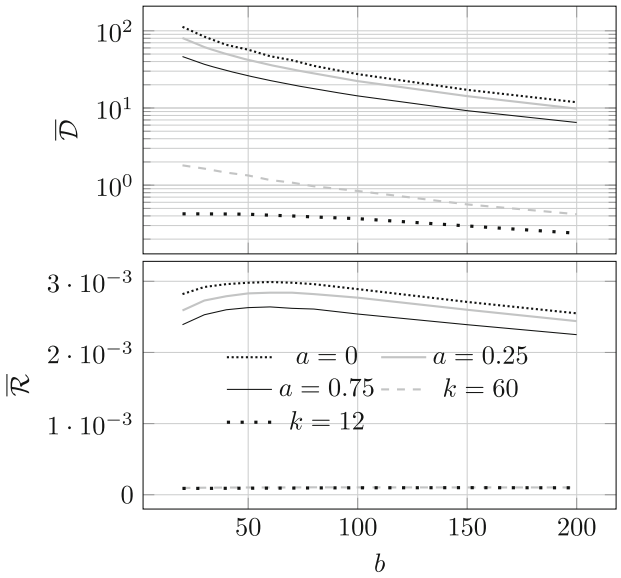


Fig. 20 Repeatability plots v.s. parameter b. The fixed-level detector returns the highest repeatability curve while $k = 12$ returns the lowest repeatability curve

the threshold b. (Recall that $a = 0$ here.) The results are obtained by averaging over a full sequence from the Oxford dataset. The number of repeatable detections is increased with decreased threshold levels while relative repeatability is approximately the same, which indicates redundant detections. Setting $b = 55$ always gives the highest repeatability for a given r. Figure 18 shows this more clearly. Here we see there is an agreement between estimation performance plots (Fig. 15) and normalized repeatability plots (Fig. 18) to have the best scores at threshold levels slightly greater than 50, independent on r.

Figure 19 shows the repeatability plots vs. r for different detectors and parameter selection on the same axis (BFAR-1-30 means $a = 1$ and $b = 30$, CFAR-2 means $a = 2$ and $b = 0$, and fixed-30 means $a = 0$ and $b = 30$). Clearly, the BFAR scores closely approach, yet remain slightly below the fixed-level scores. However, Sect. 5.4 demonstrates that it excels in odometry estimation results. This may be attributed to the greater number of redundant detections produced by the fixed-level detector, as depicted earlier in Fig. 17. CFAR reported the lowest scores, which is not surprising given the low estimation scores obtained compared to others (see Fig. 16). We select the value of $r = 5$ cm to produce Fig. 20. Notice that, fixed-level, k-strongest, and BFAR all have a similar approach to ignore targets below a certain minimum level (the parameter b in Fig. 20) so it was possible to plot the repeatability plots vs. that level. It is clear from the plots that k-strongest has the lowest repeatability scores due to the conservative nature of the filter, though it still has good estimation scores. Comparing Fig. 20 with Fig. 14 we see that BFAR repeatability is slightly increasing with increased values of b till values of b around 50, then it is decreasing slightly afterward, while we have the estimation score for BFAR is the best compared to fixed-level for values of $b < 50$. We conclude that BFAR has better estimation errors compared to other methods while maintaining good repeatability scores compared to k-strongest. The fixed-level detector works well but suffers from redundant detections and k-strongest has good estimation errors and returns more stable detections but suffers from low repeatability scores.

6 Conclusion

This paper focuses on improving radar detection algorithms (i.e., separating signal returns corresponding to actual surface detections from noise), in particular for the use case of radar-only odometry estimation. We have proposed a new detector called BFAR and showed that, compared to CA-CFAR, its parameters can be easily trained such that it keeps relevant detections and removes radar noise.

In particular, we have demonstrated the usefulness of BFAR by incorporating it in the CFEAR pipeline for radar odometry, which stands among the lowest published odometry errors in the Oxford Radar RobotCar dataset. Using the classical CA-CFAR detector with CFEAR will not lead to acceptable performance and the pipeline may fail. However, it was possible to achieve even smaller estimation errors than the original CFEAR when using our new BFAR detector instead of the baseline k-strongest detector. It was possible to reduce the estimation translation/rotation errors in CFEAR from 1.76%/0.5°/100m to 1.55%/0.46°/100m.

Conceptually, BFAR can be seen as an optimized combination between CA-CFAR and a fixed-level threshold to minimize the odometry estimation error. The structure of BFAR makes it possible to use many variants of CFAR to add their advantages, not necessarily the classical CA-CFAR that we used here for simplicity and proof of concept. Finally, even though the BFAR detector has been proposed specifically for spinning radar odometry estimation, it is expected to contribute in signal detection for other tasks and sensors with similar noise issues.

Author Contributions Anas Alhashimi authored the primary manuscript text and figures and led the experimentation work. Daniel Adolfsson contributed to the development and maintenance of the CFEAR code. All authors contributed to discussing the evaluation methodology and outcomes and reviewing the text.

Funding Open access funding provided by Örebro University. No external funding was received for this research.

Data availability The data used in this study are publicly available datasets, Oxford (Barnes et al., 2020b) and Mulran (Kim et al., 2020).

Declarations

Conflict of interest The authors declare that they have no conflict of interest.

Ethics approval As this study utilized publicly available datasets and did not involve human participants or sensitive data, ethics approval was not required.

Open Access This article is licensed under a Creative Commons Attribution 4.0 International License, which permits use, sharing, adaptation, distribution and reproduction in any medium or format, as long as you give appropriate credit to the original author(s) and the source, provide a link to the Creative Commons licence, and indicate if changes were made. The images or other third party material in this article are included in the article's Creative Commons licence, unless indicated otherwise in a credit line to the material. If material is not included in the article's Creative Commons licence and your intended use is not permitted by statutory regulation or exceeds the permitted use, you will need to obtain permission directly from the copyright holder. To view a copy of this licence, visit http://creativecommons.org/licenses/by/4.0/.

References

Adolfsson, D., Karlsson, M., Kubelka, V., et al. (2023). TBV radar SLAM—trust but verify loop candidates. IEEE Robotics and Automation Letters, 8(6), 3613–3620. https://doi.org/10.1109/LRA.2023.3268040

Adolfsson, D., Magnusson, M., Alhashimi, A., et al. (2021). CFEAR radarodometry – conservative filtering for efficient and accurate radar odometry. In *IROS* (pp. 5462–5469). https://doi.org/10.1109/IROS51168.2021.9636253

Adolfsson, D., Magnusson, M., Alhashimi, A., et al. (2022). Lidar-level localization with radar? The CFEAR approach to accurate, fast, and robust large-scale radar odometry in diverse environments. *IEEE Transactions on Robotics, 39*(2), 1–20. https://doi.org/10.1109/TRO.2022.3221302

Aldera, R., De Martini, D., Gadd, M., et al. (2019a). Fast radar motion estimation with a learnt focus of attention using weak supervision. In *2019 international conference on robotics and automation (ICRA)* (pp. 1190–1196). IEEE.

Aldera, R., De Martini, D., Gadd, M., et al. (2019b). What could go wrong? Introspective radar odometry in challenging environments. In *2019 IEEE intelligent transportation systems conference (ITSC)* (pp. 2835–2842). IEEE.

Aldera, R., Gadd, M., De Martini, D., et al. (2022). What goes around: Leveraging a constant-curvature motion constraint in radar odometry. *IEEE Robotics and Automation Letters, 7*(3), 7865–7872. https://doi.org/10.1109/LRA.2022.3186757

Barnes, D., Gadd, M., Murcutt, P., et al. (2020a). The oxford radar robotcar dataset: A radar extension to the oxford robotcar dataset. In *2020 IEEE international conference on robotics and automation (ICRA)* (pp. 6433–6438). IEEE.

Barnes, D., Gadd, M., Murcutt, P., et al. (2020b). The oxford radar robotcar dataset: A radar extension to the Oxford robotcar dataset. In *Proceedings of the IEEE international conference on robotics and automation (ICRA)*, Paris, https://arxiv.org/abs/1909.01300

Barnes, D., & Posner, I. (2020). Under the radar: Learning to predict robust keypoints for odometry estimation and metric localisation in radar. In *2020 IEEE international conference on robotics and automation (ICRA)* (pp 9484–9490). IEEE.

Barnes, D., Weston, R., & Posner, I. (2020c). Masking by moving: Learning distraction-free radar odometry from pose information. In Kaelbling, L. P., Kragic, D., & Sugiura, K. (Eds.), CoRL (Vol. 100, pp. 303–316). PMLR.

Behley, J., & Stachniss, C. (2018). Efficient surfel-based SLAM using 3D laser range data in urban environments. In *Systems (RSS)*.

Boroson, E. R., & Ayanian, N. (2019). 3d keypoint repeatability for heterogeneous multi-robot SLAM. In *2019 international conference on robotics and automation (ICRA)* (pp. 6337–6343). IEEE.

Brooker, G., Hennessey, R., Lobsey, C., et al. (2007). Seeing through dust and water vapor: Millimeter wave radar sensors for mining applications. *Journal of Field Robotics, 24*(7), 527–557.

Burnett, K., Yoon, D. J., Schoellig, A. P., et al. (2021). Radar odometry combining probabilistic estimation and unsupervised feature learning. In: Proc. of Robotics: Science and Systems (RSS). https://doi.org/10.15607/RSS.2021.XVII.029

Cen, S. H., & Newman, P. (2018). Precise ego-motion estimation with millimeter-wave radar under diverse and challenging conditions. In *2018 IEEE International Conference on Robotics and Automation (ICRA)* (pp. 1–8). IEEE.

Cen, S. H., & Newman, P. (2019). Radar-only ego-motion estimation in difficult settings via graph matching. In *2019 international conference on robotics and automation (ICRA)* (pp. 298–304). IEEE.

Finn, H. (1968). Adaptive detection mode with threshold control as a function of spatially sampled clutter-level estimates. *RCA Rev, 29*, 414–465.

Gandhi, P. P., & Kassam, S. A. (1988). Analysis of CFAR processors in nonhomogeneous background. *IEEE Transactions on Aerospace and Electronic systems, 24*(4), 427–445.

Geiger, A., Lenz, P., & Urtasun, R. (2012). Are we ready for autonomous driving? The KITTI vision benchmark suite. In *Pattern recognition (CVPR)*.

Hong, Z., Petillot, Y., Wallace, A., et al. (2021). Radar SLAM: A robust slam system for all weather conditions. https://doi.org/10.48550/ARXIV.2104.05347, https://arxiv.org/abs/2104.05347

Hong, Z., Petillot, Y., & Wang, S. (2020). RadarSLAM: Radar based large-scale SLAM in all weathers. In *2020 (IROS)* (pp. 5164–5170). https://doi.org/10.1109/IROS45743.2020.9341287

Kallasi, F., & Rizzini, D. L. (2016). Efficient loop closure based on FALKO LIDAR features for online robot localization and mapping. In *2016 IEEE/RSJ international conference on intelligent robots and systems (IROS)* (pp. 1206–1213). IEEE.

Kim, G., Park, Y. S., Cho, Y., et al. (2020). MulRan: Multimodal range dataset for urban place recognition. In *ICRA* (pp. 6246–6253). https://doi.org/10.1109/ICRA40945.2020.9197298

Kung, P. C., Wang, C. C., & Lin, W. C. (2021). A normal distribution transform-based radar odometry designed for scanning and automotive radars. In: 2021 IEEE International Conference on Robotics and Automation (ICRA), pp 14417–14423. https://doi.org/10.1109/ICRA48506.2021.9561413

Machado-Fernández, J. R., Mojena-Hernández, N., & JdlC, Bacallao-Vidal. (2017). Evaluation of CFAR detectors performance. *Iteckne, 14*(2), 170–178.

Maddern, W., Pascoe, G., Linegar, C., et al. (2017). 1 Year, 1000km: The Oxford RobotCar Dataset. *The International Journal of Robotics Research (IJRR), 36*(1), 3–15. https://doi.org/10.1177/0278364916679498

Marck. J. W., Mohamoud. A,, vd Houwen, E., et al. (2013). Indoor radar SLAM: A radar application for vision and GPS denied environments. In *2013 European radar conference* (pp. 471–474). IEEE.

Mielle, M., Magnusson, M., & Lilienthal, A. J. (2019). A comparative analysis of radar and lidar sensing for localization and mapping. In *2019 European conference on mobile robots (ECMR)* (pp. 1–6). IEEE.

Nielsen, K., & Hendeby, G. (2023). Survey on 2D LIDAR feature extraction for underground mine usage. *IEEE Transactions on Automation Science and Engineering, 20*(2), 981–994.

Park, Y.S., Shin, Y.S., & Kim, A. (2020). Pharao: Direct radar odometry using phase correlation. In *2020 IEEE international conference on robotics and automation (ICRA)* (pp. 2617–2623). IEEE.

Rey-Otero, I., Delbracio, M., & Morel, J. M. (2015). Comparing feature detectors: A bias in the repeatability criteria. In *2015 IEEE international conference on image processing (ICIP)* (pp. 3024–3028). IEEE.

Rey-Otero, I., & Delbracio, M. (2015). Is repeatability an unbiased criterion for ranking feature detectors? *SIAM Journal on Imaging Sciences, 8*(4), 2558–2580.

Tuytelaars, T., Mikolajczyk, K., et al. (2008). Local invariant feature detectors: A survey. *Foundations and Trends® in Computer Graphics and Vision, 3*(3), 177-280

Usman, M., Khan, A. M., Ali, A., et al. (2019). An extensive approach to features detection and description for 2-d range data using active b-splines. *IEEE Robotics and Automation Letters, 4*(3), 2934–2941.

Venon, A. G., Dupuis, Y., Vasseur, P., et al. (2022). Millimeter wave FMCW radars for perception, recognition and localization in automotive applications: A survey. *IEEE Transactions on Intelligent Vehicles, 7*(3), 533–555.

Weston, R., Gadd, M., De Martini, D., et al. (2022). Fast-MbyM: Leveraging translational invariance of the Fourier transform for efficient and accurate radar odometry. In *2022 international conference on robotics and automation (ICRA)* (pp. 2186–2192). https://doi.org/10.1109/ICRA46639.2022.9812063

Weston, R., Jones, O. P., & Posner, I. (2021). There and back again: Learning to simulate radar data for real-world applications. In *2021 IEEE international conference on robotics and automation (ICRA)* (pp. 12809–12816). IEEE.

Zhang, J., & Singh, S. (2017). Low-drift and real-time lidar odometry and mapping. *Autonomous Robots, 41*, 401–416. https://doi.org/10.1007/s10514-016-9548-2

Zhou, Y., Liu, L., Zhao, H., et al. (2022). Towards deep radar perception for autonomous driving: Datasets, methods, and challenges. *Sensors, 22*(11), 4208.

Publisher's Note Springer Nature remains neutral with regard to jurisdictional claims in published maps and institutional affiliations.



Anas Alhashimi is a Senior Lecturer in Computer Engineering and an active researcher in control and robotics. He completed his PhD in Automatic Control at Luleå University of Technology in 2018, following his Bachelor's (1999) and MSc degrees (2002) in Electronic and Communications Engineering. His research interests include robot perception, statistical sensor modeling and calibration, parameter estimation and model order selection under variable noise variance (heteroscedasticity), joint parameter and state estimation (for both linear and nonlinear systems), as well as robot localization, mapping, and path planning.



Daniel Adolfsson received his PhD degree in Computer Science from Örebro University in 2023. He obtained his MSc degree in Robotics from Mälardalen University, Sweden, in 2016. His research interests include robust methods for radar SLAM and large-scale localization in prior maps.



Henrik Andreasson research interest lies mainly in perception aspects ranging from people detection in harsh industrial environments to mapping and localization with a focus on industrial vehicles. He also has an interest in navigation and fleet coordination, more specifically in combining motion planning and control for single and multiple vehicles. He completed his undergraduate studies at the Royal Institute of Technology (KTH) and obtained his PhD from Örebro University.



Achim Lilienthal is full professor, head of the chair "Perception for Intelligent Systems", and manager of the "KI.Fabrik" at the German Museum in Munich. His research fundamentally targets perception systems in unconstrained, dynamic environments. Typically leveraging domain knowledge and AI, his research addresses mobile robot olfaction, rich 3D perception, navigation of autonomous mobile robots, human-robot interaction, etc. He obtained his Ph.D. with a thesis about mobile robot olfaction at Tübingen University. He has been the coordinator of three EU projects and PI in six EU projects, established two spinoff companies in Sweden (Retenua and QTPIE), has published more than 300 refereed conference papers and journal articles, is senior member of IEEE, and evaluator for several national funding agencies and the EU.



Martin Magnusson is an associate professor (docent) in computer science at the MRO lab, Örebro University. He received his MSc degree in computer science from Uppsala University in 2004 and PhD degree from Örebro University in 2009. His research interests include 3D perception (including efficient and versatile 3D surface representations), creation and usage of flow-aware and reliability-aware robot maps that go beyond mere geometry, and methods for making use of heterogeneous maps with high uncertainty.